Ground motion estimation for the elevated bridges of the Kyushu Shinkansen derailment caused by the foreshock of the 2016 Kumamoto earthquake based on the site-effect substitution method

AUTHOR(S):

Hata, Yoshiya; Yabe, Masaaki; Kasai, Akira; Matsuzaki, Hiroshi; Takahashi, Yoshikazu; Akiyama, Mitsuyoshi

CITATION:

Hata, Yoshiya ...[et al]. Ground motion estimation for the elevated bridges of the Kyushu Shinkansen derailment caused by the foreshock of the 2016 Kumamoto earthquake based on the site-effect substitution method. Earth, Planets and Space 2016, 68: 199.

ISSUE DATE:

2016-12-01

URL:

http://hdl.handle.net/2433/218892

Hata *et al. Earth, Planets and Space* (2016) 68:199
DOI 10.1186/s40623-016-0573-3

Earth, Planets and Space

LETTER Open Access

Ground motion estimation for the elevated bridges of the Kyushu Shinkansen derailment caused by the foreshock of the 2016 Kumamoto earthquake based on the site-effect substitution method

Yoshiya Hata[1*], Masaaki Yabe[2], Akira Kasai[3], Hiroshi Matsuzaki[4], Yoshikazu Takahashi[5] and Mitsuyoshi Akiyama[6]

Abstract

An earthquake of JMA magnitude 6.5 (first event) hit Kumamoto Prefecture, Japan, at 21:26 JST, April 14, 2016. Subsequently, an earthquake of JMA magnitude 7.3 (second event) hit Kumamoto and Oita Prefectures at 01:46 JST, April 16, 2016. An out-of-service Kyushu Shinkansen train carrying no passengers traveling on elevated bridges was derailed by the first event. This was the third derailment caused by an earthquake in the history of the Japanese Shinkansen, after one caused by the 2004 Mid-Niigata Prefecture Earthquake and another triggered by the 2011 Tohoku Earthquake. To analyze the mechanism of this third derailment, it is crucial to evaluate the strong ground motion at the derailment site with high accuracy. For this study, temporary earthquake observations were first carried out at a location near the bridge site; these observations were conducted because although the JMA Kumamoto Station site and the derailment site are closely located, the ground response characteristics at these sites differ. Next, empirical site amplification and phase effects were evaluated based on the obtained observation records. Finally, seismic waveforms during the first event at the bridge site of interest were estimated based on the site-effect substitution method. The resulting estimated acceleration and velocity waveforms for the derailment site include much larger amplitudes than the waveforms recorded at the JMA Kumamoto and MLIT Kumamoto station sites. The reliability of these estimates is confirmed by the finding that the same methods reproduce strong ground motions at the MLIT Kumamoto Station site accurately. These estimated ground motions will be useful for reasonable safety assessment of anti-derailment devices on elevated railway bridges.

Keywords: Seismic observation, Site-effect, Response spectrum

Introduction

Beginning on April 14, 2016, a series of damaging earthquakes hit Kumamoto and Oita Prefectures in Kyushu, Japan. This series began with the *M*w 6.2 event (April 14, 21:26 JST; hereafter referred to as the foreshock, although the source faults of the foreshock and the main shock are not identical), followed by the *M*w 7.0 main shock (April 16, 1:25 JST). As of June 30, this sequence involved more than 1800 perceptible earthquakes (Japan Meteorological Agency (JMA) 2016). The entire sequence was named the "2016 Kumamoto earthquake" by the JMA.

The 2016 Kumamoto earthquake sequence has exposed a potential weakness of Japanese Shinkansen train technology by disrupting the operations of the Kyushu Shinkansen Line. A train was derailed by strong ground motion, which was measured as seven on the Japanese intensity scale at the Mashiki Town Office (Hata et al. 2016a; see Fig. 1; Table 1). The bullet train was bound

*Correspondence: hata@civil.eng.osaka-u.ac.jp
[1] Graduate School of Engineering, Osaka University, 2-1 Yamada-oka, Suita, Japan
Full list of author information is available at the end of the article

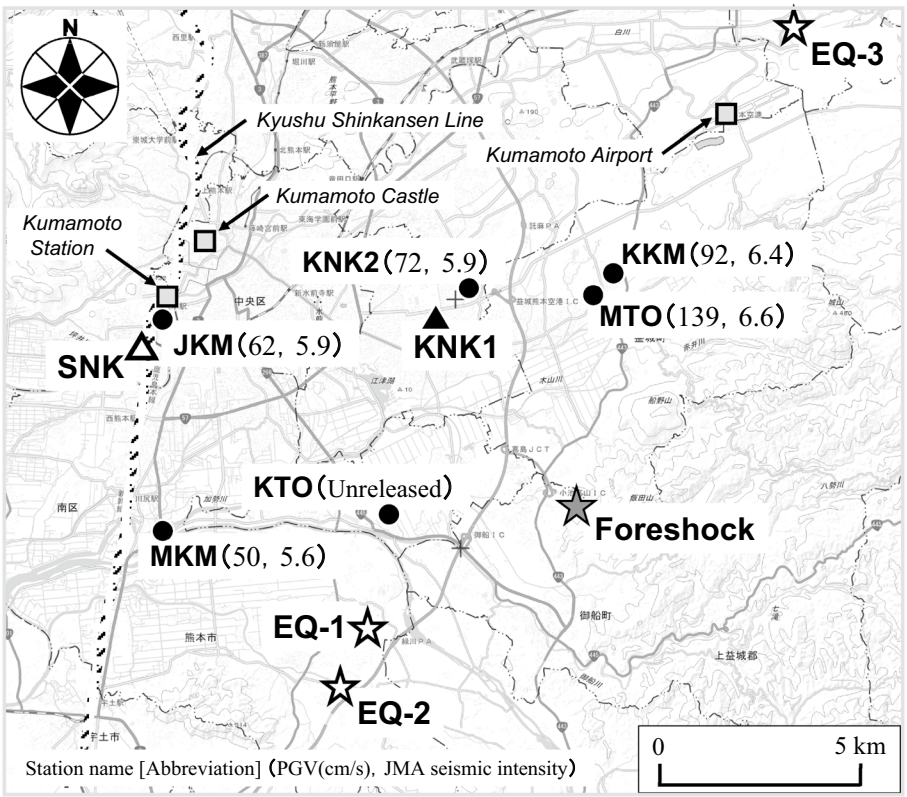

Fig. 1 Observation results of strong ground motions around SNK during the foreshock of the 2016 Kumamoto earthquake. Peak ground velocities (in cm/s) are composites of three components; JMA seismic intensity was calculated from these composites values. *Stars* indicate the epicenters of the foreshock and the moderate events recorded during the temporary observations; *circles* represent the permanent station sites for strong motion observation. The strong motion stations are listed in Table 1. *Source* parameters of the foreshock and the moderate events are listed in Table 2

Table 1 List of strong motion stations

Abbreviation	Station name
SNK	Derailment site of Kyushu Shinkansen (temporary earthquake observation site)
JKM	JMA Kumamoto
MKM	MLIT Kumamoto
KTO	Kashima Town Office
KNK1	K-NET Kumamoto [past] (temporary earthquake observation site)
KNK2	K-NET Kumamoto (present)
MTO	Mashiki Town Office
KKM	KiK-net Mashiki

for a rail yard at a speed of 80 km/h after completing a commercial service at the JR Kumamoto Station. Fortunately, no passengers were onboard the bullet train, and the operator was not injured (Ministry of Land, Infrastructure, Transport and Tourism (MLIT) 2016). However, if the bullet train had been carrying passengers and traveling at a higher speed, it could have resulted in a major disaster. Generally, Shinkansen lines are equipped with a system to detect preliminary tremors and stop the bullet trains. However, as this derailment shows, this system may not work when earthquakes occur close to the rail lines (see Fig. 1). Moreover, this event was the third derailment caused by an earthquake in the history of the Japanese Shinkansen, after one caused by the 2004 Mid-Niigata Prefecture Earthquake (Ogura 2006) and another triggered by the 2011 Tohoku Earthquake (Horika 2013).

To analyze the mechanism of this third derailment, it is crucial to evaluate the strong ground motion at the derailment site with high accuracy. For this study, strong motion estimation was carried out at the derailment site with consideration for empirical site amplification and phase effects. First, temporary earthquake observations were conducted at the derailment site. Then, ground shaking characteristics at the derailment site were evaluated based on the obtained records. In addition, strong ground motions at the derailment site during the foreshock were evaluated based on the site-effect

substitution method (Hata et al. 2011). The same method was also applied to estimate strong ground motions at a nearby strong motion station, where the foreshock ground motion was observed, to investigate the applicability of this method to this particular earthquake. The estimated ground motions were highly consistent with the observed ground motions, which indicate the applicability of this estimation method. Finally, the response spectra of the evaluated strong motions at the derailment site were compared with the design response spectrum of the Specifications for Railway Structures (Railway Technical Research Institute (RTRI) 1999) based on an effect of very soft ground (G5 ground; RTRI 2012).

Observed ground motions

In Kumamoto Prefecture, a strong motion observation network with high density was formed by the National Research Institute for Earth Science and Disaster Resilience (Aoi et al. 2004), the JMA (Nishimae 2004), the MLIT (Uehara and Kusakabe 2004), and the local government (Kumamoto Prefecture 2015). Thus, a large number of strong motion records were obtained during the foreshock. The locations of the strong motion stations around the derailment site, as well as observed peak ground velocities (PGVs) and JMA seismic intensities (Nishimae 2004), are shown in Fig. 1. A list of the stations and their abbreviations are provided in Table 1. Thus, strong motion records are generally available for the area around the derailment site. However, strong ground motions can vary significantly due to variations in local geology (e.g., Hata et al. 2014). Therefore, it is important to estimate the properties of strong ground motions at the site of interest taking into account the effects of local geology (i.e., site effects). Figure 2 shows the detailed locations of the stations SNK and JKM (see Table 1). Although the derailment caused by the foreshock was observed at SNK, serious damage to the elevated bridges was not observed around JKM, based on the authors' field reconnaissance.

Conventional estimation methods

Conventional approaches to estimate strong ground motions after an earthquake at a site of interest based on moderate earthquake records fall into two categories. One of these categories is based on full strong motion simulation using fault models and moderate earthquake records as empirical Green's functions (e.g., Suzuki and Iwata 2006). In these approaches, because the time history of strong ground motion is generated, one can obtain ground motion parameters such as peak amplitude and duration. However, the reliability of the results from these approaches depends on the quality of the fault model, and it may not always be possible to obtain a sufficiently reliable model.

For the second category, a practical estimation method for strong ground motions (called the "site-effect substitution method") was proposed by Hata et al. (2011). This method is based on records of moderate earthquakes at both the site of interest and a nearby permanent strong motion observation station, and on a record of a large earthquake at the nearby station. Because this method is focused not only on the difference in site amplification factors but also on the difference in site phase effects between the site of interest and the nearby station, it can be used to compute time histories of strong ground motions at the site of interest with high accuracy (e.g., Hata et al. 2013, 2016b). Because JKM is located close to SNK, as shown in Figs. 1 and 2, this method is accepted as suitable for this study.

Another advantage of this method is its simplicity. Unlike full strong motion calculations, such as those based on the Stochastic Green's Function Method (e.g., Hata et al. 2012), this method does not require a fault model for the large event. Therefore, it can be applied at an early stage of the response to a large event even if a reliable fault model is not yet available. Because the fault

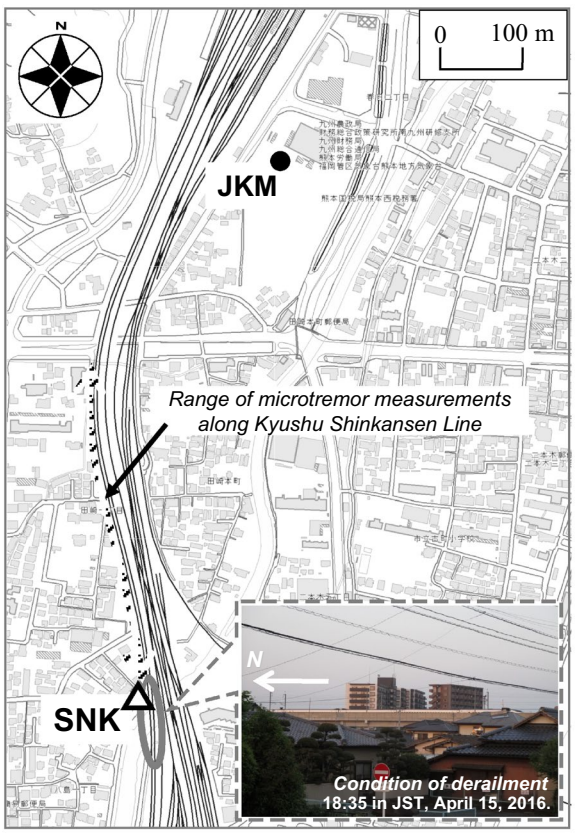

Fig. 2 Detailed location map of SNK and JKM. The locations of the observation stations are plotted on a topographic map from the Geospatial Information Authority of Japan. The shortest distance between the stations is about 700 m

models for this earthquake are still under development, we have used the site-effect substitution method (Hata et al. 2011) to estimate strong ground motions in this study.

Temporary earthquake observation

During the 2016 Kumamoto earthquake sequence, in addition to the damage caused by the main shock, damage from the foreshock was significant. In particular, during the reconnaissance survey conducted on April 15, the location of the derailment was found just to the south of the JR Kumamoto Station (see Fig. 2).

To reveal the cause of the derailment and analyze the wavefield, the authors deployed a seismic array with two temporary stations, as shown in Fig. 1. As indicated in Fig. 1 and Table 1, the station SNK is located in the derailment area close to the station JKM. More specifically, the actual derailment of the train must have occurred at a point a certain distance from SNK before the train stopped at SNK. However, the actual location of the derailment is not clear (MLIT 2016). Therefore, considering the speed of the bullet train (80 km/h), we carried out microtremor measurements at eight sites along the elevated bridges at intervals of approximately 50 m. Figure 3 shows a comparison of the microtremor H/V spectra of SNK and the other seven sites. Based on the results shown in Fig. 3, we confirmed the similarity of these H/V spectra, which suggests that the site effects evaluated based on the temporary observations could be applied for the region covered by the microtremor observations. The station KNK1 is located at the former K-NET Kumamoto site, which is close to its present location at KNK2 (Hata et al. 2016c). Note that the K-NET Kumamoto (KMM006) site was relocated to KNK2 from KNK1 on March 13, 2015. The period of both observations was almost nine hours, beginning at 18:00 JST on April 15, 2016. Observations were recorded at KNK1 because the empirical site amplification factor was available for this site (Nozu et al. 2007), and the site was intended to be used as a reference site, as described in the following sections. A servo-type accelerometer JU-210 (Senna et al. 2006) was installed at SNK and KNK1. The accelerometer was fixed to the ground with an anchor at each station. Continuous observation was conducted for three components with a sampling frequency of 100 Hz. The timing of the accelerometer measurements was synchronized via GPS.

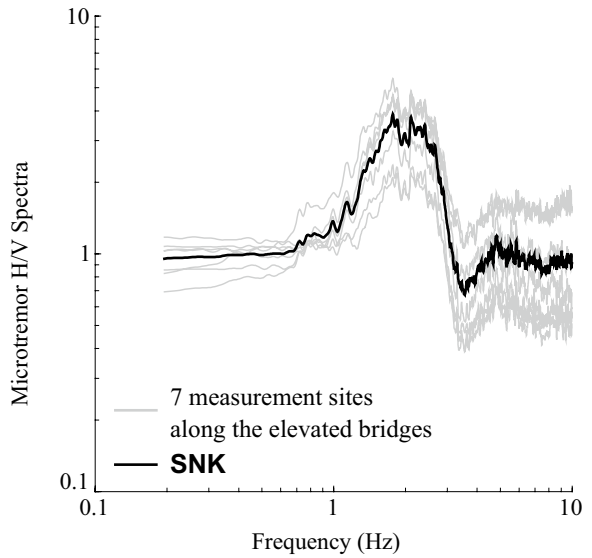

Fig. 3 Comparison of the microtremor H/V spectra for evaluating the applicability of the temporary earthquake observation site created at SNK

Table 2 lists the observed earthquake events at SNK and KNK1. EQ-1, EQ-2, and EQ-3 were moderate earthquakes that originated within the source region of the foreshock and were used to evaluate the site amplification factor at SNK. The source parameters and earthquake mechanisms of the foreshock and EQ-1–3 are also listed in Table 2. EQ-2 was used for the evaluation of the site phase effect at SNK because of its location near that of the foreshock. The earthquake focal mechanisms of the foreshock and EQ-2 were also similar (see Table 2). Because EQ-2 was the only event that was recorded at SNK and MKM, its records were used to evaluate the applicability of the site-effect substitution method. Figure 4 shows the observed acceleration waveforms at the ground surface at MKM and SNK associated with EQ-2; the differences in seismic waveforms and peak accelerations between MKM and SNK are confirmed by these results.

Site amplification factor

The horizontal site amplification factors for the K-NET stations, including the former K-NET Kumamoto station (KNK1), have previously been evaluated by Nozu et al. (2007) based on spectral inversion. However, the site amplification factors for the JMA stations, MLIT stations, and SNK have not been previously reported. In this study, the spectral ratio method (Hata et al. 2014) was applied to evaluate the horizontal site amplification factors at JKM, MKM, and SNK. This method was performed based on moderate earthquake records obtained at the reference station and the sites of interest simultaneously. The sites of interest include JKM, MKM, and SNK. KNK1 was selected as the reference station for this study.

The procedure of the spectral ratio method is summarized as follows. For each combination of a site of interest and the reference station, the spectral ratio of the Fourier

Table 2 Parameters for the foreshock and the observed earthquake events

	Foreshock	EQ-1	EQ-2	EQ-3
Date (year/month/day)	April 14, 2016	April 15, 2016	April 15, 2016	April 15, 2016
Origin time[a] (H:Min:S)	21:26:34.43	18:48:12.70	20:15:13.50	23:17:31.62
Source region[a]	NW Kumamoto Pref.	NW Kumamoto Pref.	NW Kumamoto Pref.	NW Kumamoto Pref.
Latitude[a] (deg.)	N 32.7417	N 32.7105	N 32.6972	N 32.8598
Longitude[a] (deg.)	E 130.8087	E 130.7503	E 130.7417	E 130.8740
Depth[a] (km)	11.39	13.44	12.47	7.02
M_J [a]	6.5	3.9	3.8	3.6
M_W [b]	6.1	3.7	3.7	3.8
M_0 [b] (Nm)	1.74E + 18	4.48E + 14	4.25E + 14	5.52E + 14
(strike, dip, rake)[b] (deg.)	(212, 89, 164)	(33, 87, 162)	(207, 70, 178)	(281, 51, 59)
Focal mechanisms[b]	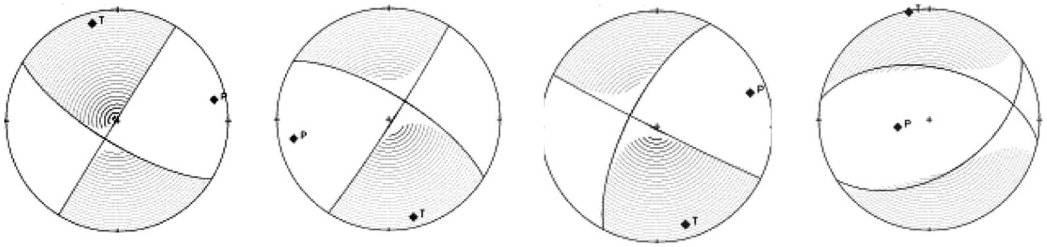			

[a] After JMA

[b] After F-net (www.fnet.bosai.go.jp)

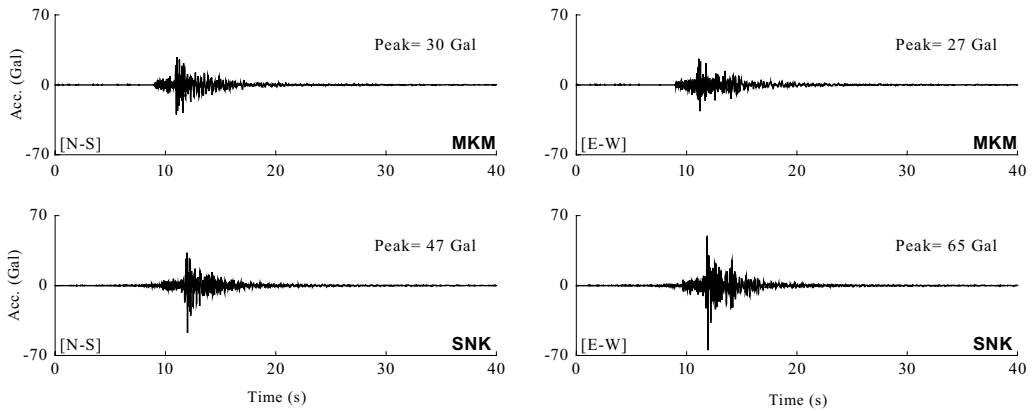

Fig. 4 Comparison of the observed acceleration waveforms that occurred during EQ-2 close to the main rupture area of the foreshock at MKM and SNK for the N–S and E–W components

amplitudes of the records from the reference station and the site of interest was calculated. Here, the moderate earthquake records from before the foreshock were used for JKM and MKM (Hata et al. 2016c, d). For SNK, the records after the foreshock were used (see Table 2). The effects of geometrical spreading and anelastic attenuation were considered as the path effect (Boore 1983) to correct the Fourier spectra. We assumed a Q value of $Q = 104\, f^{0.63}$ (Kato 2001). The mean of the corrected spectral ratios (the site of interest/the reference station) was calculated. The site amplification factor at the site of interest was obtained as the product of the site amplification factor at the reference station and the spectral ratio. Here, the frequency range for the evaluation of the site amplification factor is from 0.2 to 10 Hz because the site amplification factor at the reference station is reliable within this range (Nozu et al. 2007). It should be noted that in this scheme, the site amplification factors at JKM, MKM, and SNK represent amplification from the seismic bedrock to the ground surface.

Figure 5 shows a comparison of the site amplification factors from the seismic bedrock to the ground surface at JKM, MKM, and SNK. We also performed additional geotechnical investigations focused on the shallow soil layers from the engineering bedrock to the ground surface, including microtremor measurements, standard penetration tests, and PS logging. Table 3a shows the vertical profile of shear wave velocity at SNK. For comparison, the soil profiles at/near MKM and JKM are listed in Table 3b, c, respectively. As shown in Fig. 5 and Table 3, the soil profile characteristics and the site amplification factors at SNK are not similar to those at JKM and MKM. In particular, the site amplification factors for the horizontal components at SNK are larger than those at JKM and MKM for most frequencies, which suggests that the foreshock ground motions at SNK were different from those observed at JKM and MKM.

Ground motion estimation

Figures 6 and 7 show the concept and framework of strong motion estimation at the sites of interest (MKM and SNK) using the site-effect substitution method (Hata et al. 2011). This simple method consists of three steps. First, to remove the effect of nonlinear ground response from the engineering bedrock at a depth of 32 m (see Table 3c) to the ground surface captured in the foreshock records recorded at the ground surface at JKM (see Fig. 8a, b), linear calculation was carried out (see Fig. 6) in addition to the equivalent linear calculation with the empirical dynamic deformation properties (Yasuda and Yamaguchi 1985; Yoshida et al. 2002; Hata et al. 2016b). Then, the Fourier amplitude was calculated for the linear surface ground motions at JKM, and the results were corrected for the difference of the path effects (Boore 1983) and the site amplification factors between the sites of interest and JKM (see Fig. 5) to obtain the Fourier amplitudes for the sites of interest. We assumed a Q value of $Q = 104 f^{0.63}$ (Kato 2001).

Then, the Fourier phase during the foreshock at each site of interest was approximated as the Fourier phase at the same site during EQ-2 (see Fig. 4), which occurred close to the foreshock. Finally, an inverse Fourier transform was conducted to obtain a causal time history (Nozu et al. 2009) of strong ground motions during the foreshock at each site of interest. To consider the effect of nonlinear ground response from the engineering bedrock at a depth of 26 (see Table 3b) and 35 m (see Table 3a) to

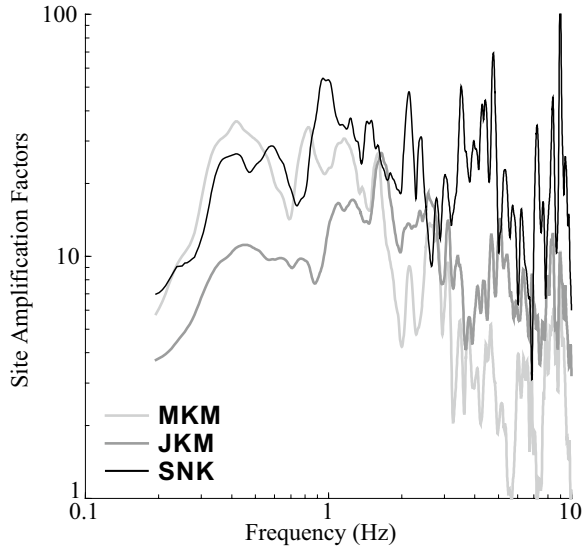

Fig. 5 Comparison of the site amplification factors in the horizontal direction at SNK, JKM, and MKM. *Note* that the spectra for JKM and MKM are based on moderate earthquake observation records from before the foreshock; the spectrum for SNK is based on temporary observation records associated with moderate earthquakes that occurred between the foreshock and the main shock (see Table 2)

Table 3 Shear wave velocity profiles at JKM, MKM, and SNK

Thickness (m)	Depth (m)	Shear wave velocity (m/s)
(a) SNK		
3.8	3.8	130
2.2	6.0	110
2.5	8.5	210
2.3	10.8	100
11.1	21.9	180
6.0	27.9	80
4.4	32.3	130
2.7	35.0	220
–	–	550
(b) MKM		
4.0	4.0	140
3.6	7.6	240
3.5	11.1	190
7.1	18.2	250
5.2	23.4	100
2.6	26.0	160
–	–	550
(c) JKM		
2.8	2.8	120
3.5	6.3	100
3.5	9.8	230
3.9	13.7	170
6.1	19.8	200
5.9	25.7	80
4.9	30.6	110
1.4	32.0	160
–	–	450

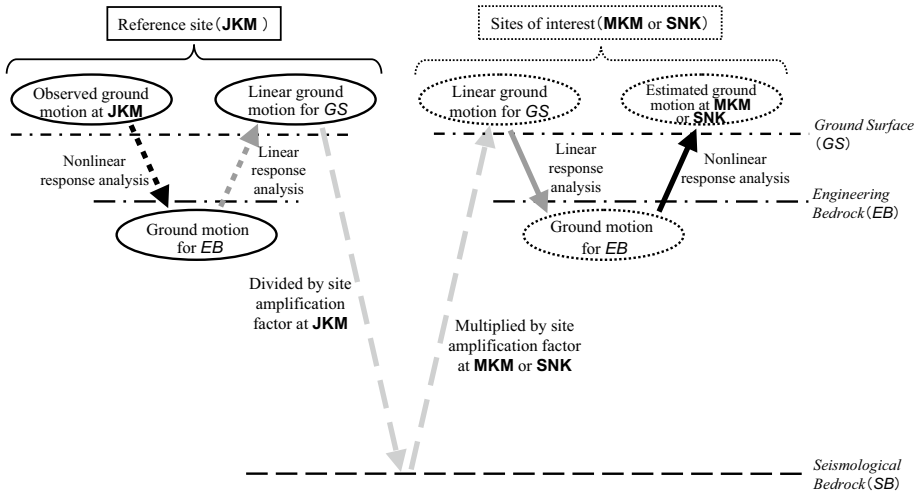

Fig. 6 Concept for the estimation of ground motions. The flow of strong ground motion estimation at MKM or SNK based on the observed strong ground motion at JKM during the foreshock is illustrated

the ground surface at MKM and SNK, respectively, not only linear calculations but also the equivalent linear calculations with the empirical dynamic deformation properties (Yasuda and Yamaguchi 1985; Yoshida et al. 2002; Hata et al. 2016b) were performed (see Fig. 6).

To confirm the validity of this estimation method, as shown in Figs. 8c, d and 9c, d, the observed acceleration and velocity waveforms (the black traces) versus the synthetic acceleration and velocity waveforms (the red traces) at MKM at the ground surface were compared.

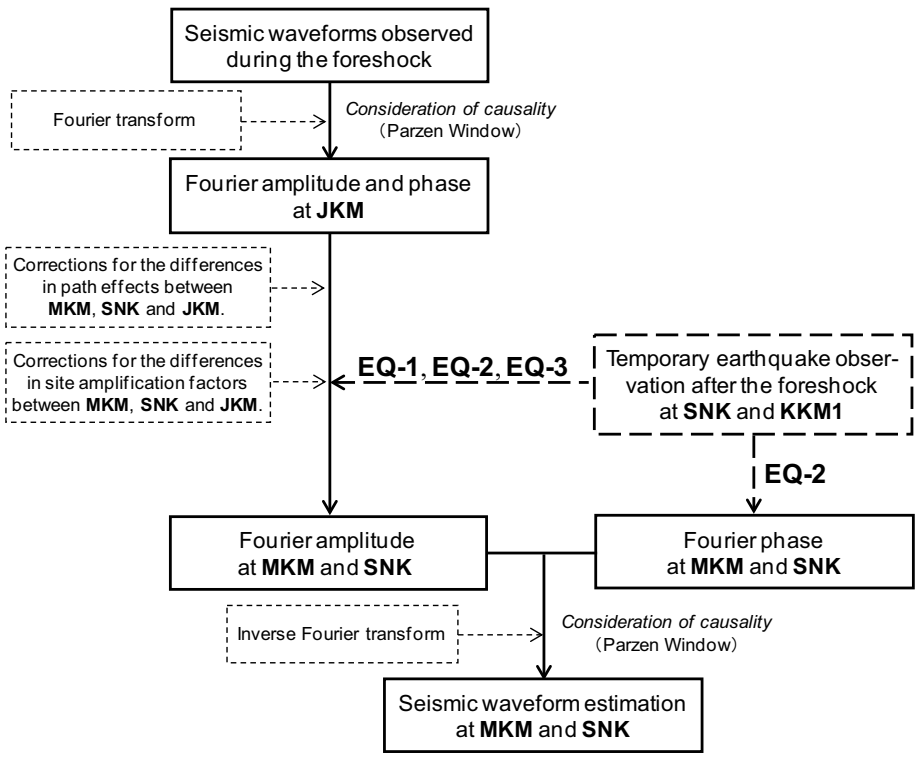

Fig. 7 Framework for estimating ground motions. MKM and SNK are the sites of interest where strong ground motions during the foreshock are to be evaluated. JKM is a nearby observation station for strong ground motions

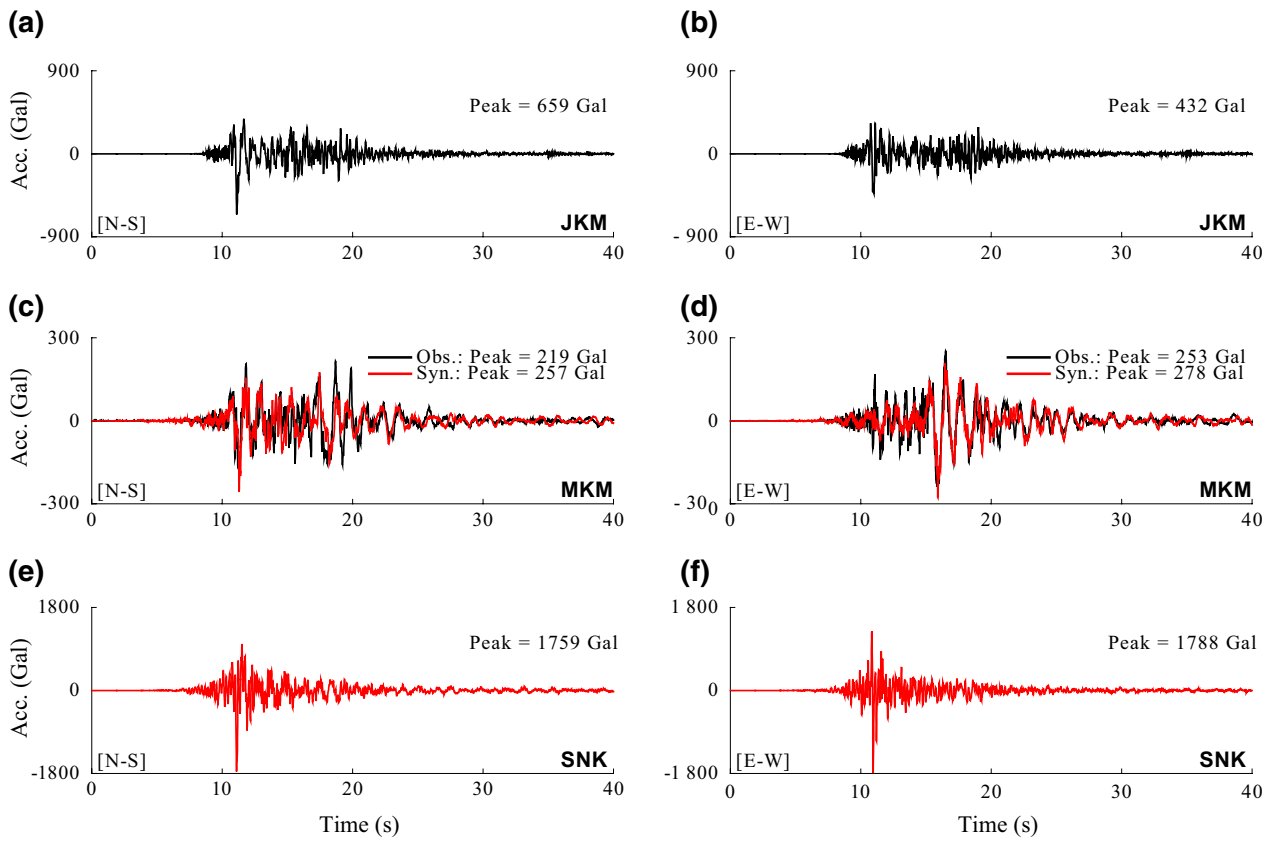

Fig. 8 The observed acceleration waveforms (*black traces*) and the estimated acceleration waveforms (*red traces*) at JKM, MKM, and SNK for the N–S and E–W components. The estimated acceleration waveforms at MKM and SNK (see **c**, **d**, **e** and **f**) were calculated based on the observed acceleration waveforms at JKM (see **a** and **b**). At MKM, the similarity between the *black traces* and *red traces* indicates the applicability of this ground motion estimation method (see **c** and **d**)

Here, not all waveforms are band-pass-filtered. Furthermore, Figs. 10c, d and 11c, d show comparisons of the response spectra (damping: 5%) based on the observed and synthetic acceleration waveforms at MKM (see Figs. 8c, d). In Figs. 8c, d, 9c, d, 10c, d and 11c, d, the similarities of all traces at MKM are confirmed, which indicates the applicability of this estimation method.

Figures 8e, f and 9e, f show the estimated acceleration and velocity waveforms, respectively, at SNK. Here, not all waveforms are band-pass-filtered. From comparison of Figs. 8a, b, e, f, a striking feature of the estimated acceleration waveforms at SNK is that these waveforms include a much larger acceleration amplitude compared to the records from JKM close to SNK. In Fig. 9a, b, e, f, again, the estimated ground motions for SNK at the ground surface include a much larger velocity amplitude compared to those for JKM. These differences in the strong ground motions may have resulted in the different responses of the elevated bridges at these sites during the foreshock. Table 4 lists the peak ground acceleration (PGA) and peak ground velocity (PGV) values at JKM and SNK. Note that the PGA and PGV values at SNK for the main shock were observed by the authors. These data confirm that at SNK, the observed PGA values for the main shock were as large as the estimated PGA values for the foreshock.

Figures 10a, b and 11a, b show the absolute acceleration spectra and the relative velocity spectra (damping: 5%) based on the observed foreshock records at JKM with respect to the design response spectrum of the Specifications for Railway Structures (RTRI 2012) and the surface ground conditions at JKM (see Table 3c). As shown in Figs. 10a, b, and 11a, b, at JKM, the observed acceleration and velocity response spectra recorded during the foreshock are almost included within the design response spectrum. This rough inclusion agrees well with the minor damage to the elevated bridge near JKM noted during the authors' field reconnaissance.

Figures 10e, f and 11e, f show the response spectra (damping: 5%) based on the estimated waveforms

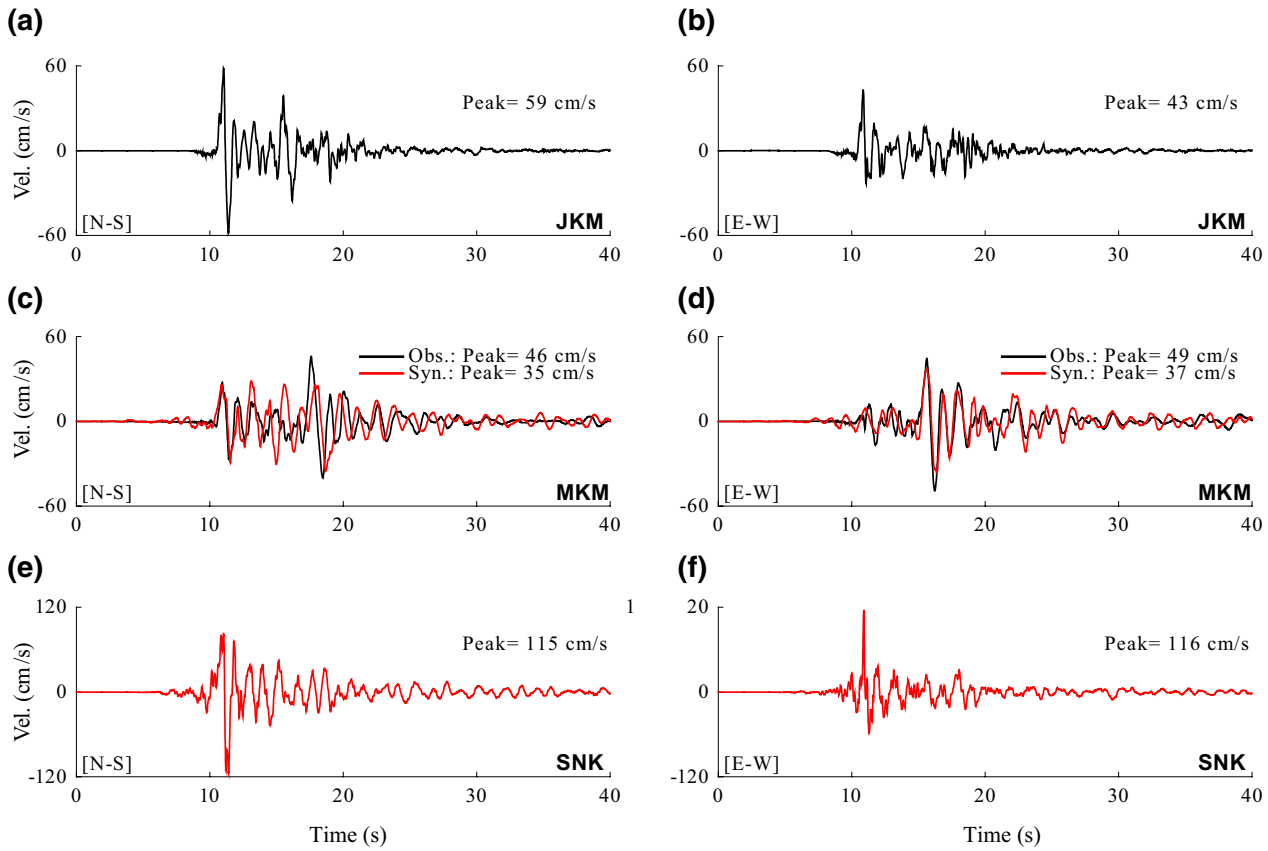

Fig. 9 The observed velocity waveforms (*black traces*) and the estimated velocity waveforms (*red traces*) at JKM, MKM, and SNK for the N–S and E–W components. The estimated velocity waveforms at MKM and SNK (see **c**, **d**, **e** and **f**) were calculated based on the observed velocity waveforms at JKM (see **a** and **b**). The velocity waveforms are without band-pass filtering. At MKM, the similarity between the *black traces* and *red traces* indicates the applicability of this ground motion estimation method (see **c** and **d**)

during the foreshock at SNK compared to the design response spectrum based on the surface ground conditions at SNK (see Table 3a). As shown in these figures, at SNK, the predominant period and the envelope of the estimated response spectra for the N–S and E–W components do not differ significantly. The estimated acceleration and velocity response spectra are larger than the design response spectrum for most natural periods from 0.1 to 1 s. Because the natural period of the elevated bridge is almost 0.7 s (Nakaaki et al. 2012; Tokunaga et al. 2015), it is likely that the inertial force on the structure during the foreshock was a main cause of the derailment on the elevated bridge. Although the estimated foreshock ground motions exceeded the design spectrum, the bridge itself was not significantly damaged by the strong ground motions. This finding may imply that these bridges can withstand strong ground motions that somewhat exceed the design spectrum, as they did during the main shock.

Summary and conclusions

During the foreshock of the 2016 Kumamoto earthquake (*M*W 6.2), a derailment occurred on an elevated bridge about 1.3 km south of the JR Kumamoto Station. In this study, strong ground motion during the foreshock at the derailment site was estimated based on empirical site amplification and phase effects. At the current stage of this study, the following conclusions have been reached.

1. Although the JMA Kumamoto Station site and the derailed bridge site are closely located, the ground response characteristics at these sites differ, which indicates differences in the local site effects at these sites and the importance of considering local site effects in estimating strong ground motions. Therefore, the local site effects at the derailment site were evaluated based on temporary earthquake observations after the foreshock associated with this event.

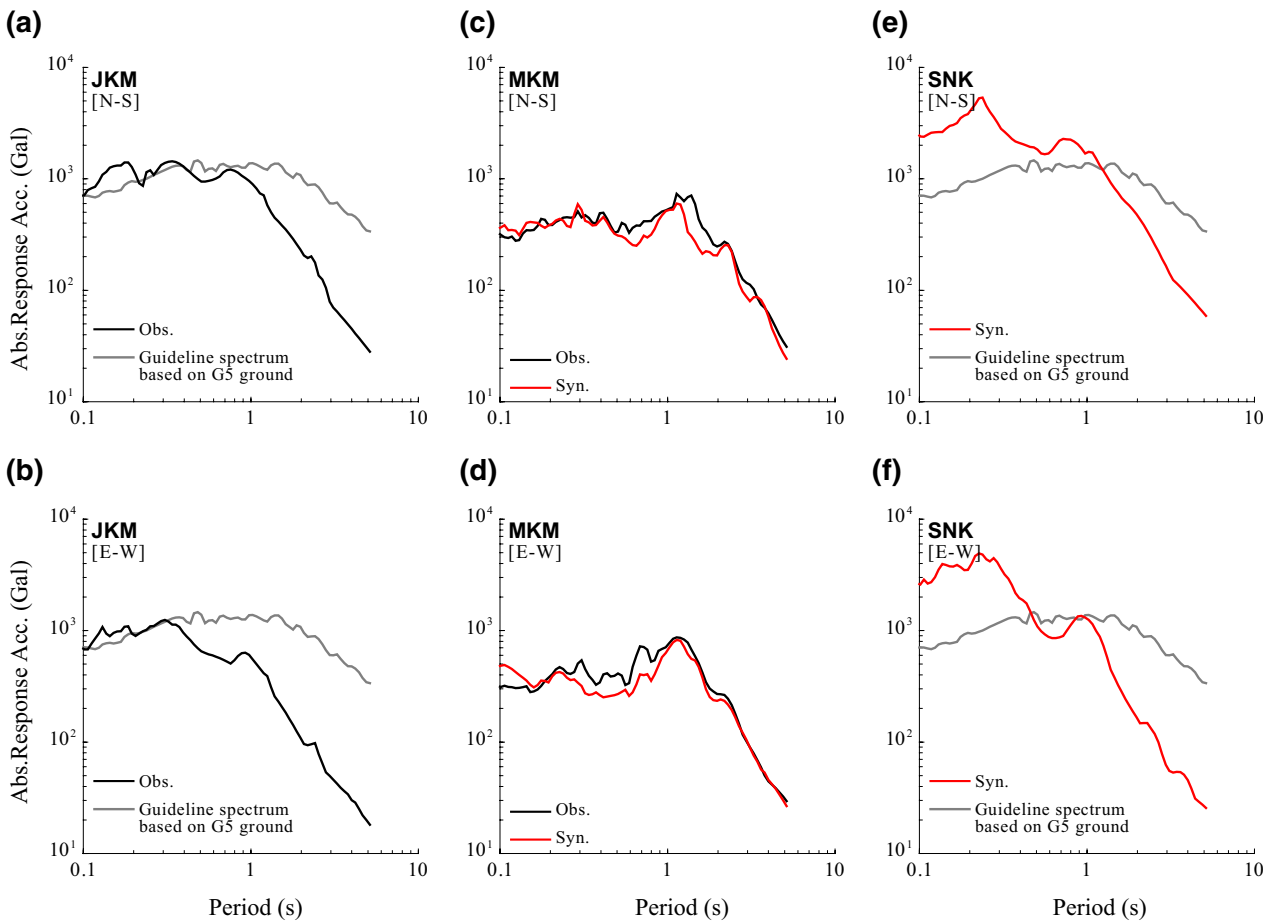

Fig. 10 The absolute acceleration response spectra calculated from the observed ground motions at JKM and MKM (*black lines*) and the estimated ground motions at MKM and SNK (*red lines*) with the guideline spectrum (*gray lines*). The damping ratio is 0.05. At MKM, the similarity between the *black traces* and *red traces* indicates the applicability of this ground motion estimation method (see **c** and **d**). At JKM, the observed response spectra are almost included within the guideline spectrum (see **a** and **b**); at SNK, the estimated response spectra exceed the guideline spectrum in the natural period range from 0.1 to 1 s (see **e** and **f**)

Table 4 PGA and PGV values at JKM and SNK during the foreshock and main shock

Event	PGA value (Gal)				PGV value (cm/s)			
	JKM		SNK		JKM		SNK	
	N–S	E–W	N–S	E–W	N–S	E–W	N–S	E–W
Foreshock	659	432	1759	1788	59	43	115	116
Main shock	606	552	1701	1382	71	41	110	75

2. A striking feature of the estimated acceleration and velocity waveforms for the foreshock at the derailment site based on the site-effect substitution method is that these waveforms include much larger amplitudes compared to the records at the permanent stations near the derailment site at the JMA Kumamoto and MLIT Kumamoto stations. The reliability of the estimations was confirmed by the fact that the same method reproduces strong ground motions at the MLIT Kumamoto station site accurately.
3. As a result of the estimation, it was found that around the natural period of the elevated bridge (0.7 s), the acceleration and velocity response spectra exceeded the design response spectrum of the Specifications for Railway Structures. Therefore, it

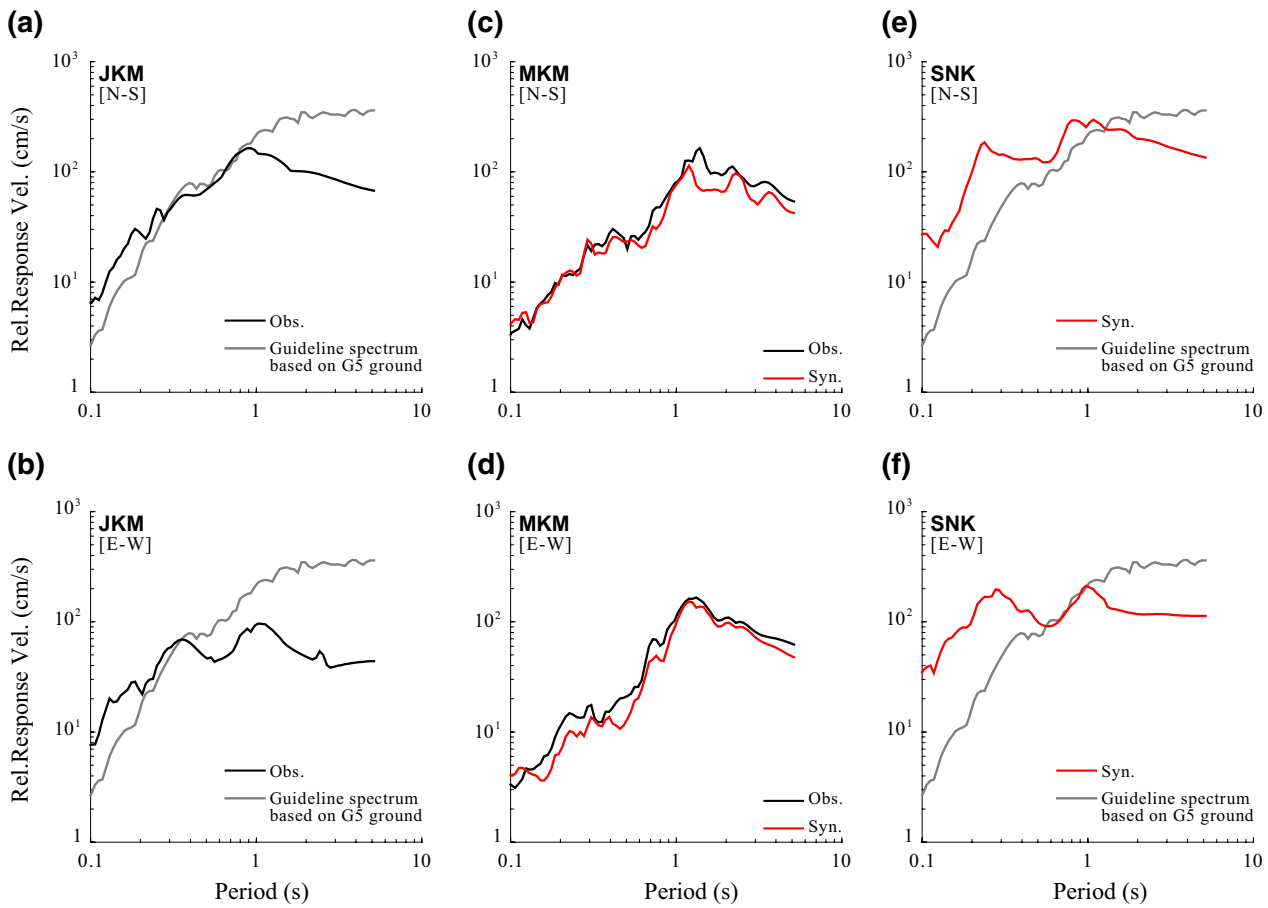

Fig. 11 The relative velocity response spectra calculated from the observed ground motions at JKM and MKM (*black lines*) and the estimated ground motions at MKM and SNK (*red lines*) with the guideline spectrum (*gray lines*). The damping ratio is 0.05. At MKM, the similarity between the *black traces* and *red traces* indicates the applicability of this ground motion estimation method (see **c** and **d**). At JKM, the observed response spectra are almost included within the guideline spectrum (see **a** and **b**); at SNK, the estimated response spectra exceed the guideline spectrum within the natural period range from 0.1 to 1 s (see **e** and **f**)

is likely that the inertial force on the structure during the foreshock was one of the main causes of the derailment on the elevated bridge.

These results suggest that it is important to take into account site-specific characteristics of strong ground motions for reasonable safety assessment of anti-derailment devices for future large earthquakes. In future study, seismic response analysis of elevated bridges for bullet trains will be carried out using estimated strong ground motions.

Data and resources

K-NET and KiK-net strong motion data were provided by the National Research Institute for Earth Science and Disaster Resilience at www.kyoshin.bosai.go.jp (last accessed July 2016). Strong motion data from the JMA network were provided by the Japan Meteorological Business Support Center on CD-ROMs and by the JMA at www.data.jma.go.jp/svd/eqev/data/kyoshin/jishin/index.html (last accessed July 2016). Strong motion data at MKM can be obtained from the Earthquake Disaster Management Division, Road Structures Department, National Institute for Land and Infrastructure Management at www.nilim.go.jp/lab/rdg/ (last accessed July 2016). Strong motion data for the foreshock were provided by the local government office of Kumamoto Prefecture at www.data.jma.go.jp/svd/eqev/data/kyoshin/jishin/160414_kumamoto/index2.html (last accessed July 2016). The Centroid Moment Tensor (CMT) solutions of the F-net were obtained from the Full Range Seismograph Network of Japan (F-net) Web site at www.fnet.bosai.go.jp (last accessed July 2016).

Authors' contributions

YH conducted the observations and estimations. YH, MY, and AK drafted the manuscript. MY, AK, and YT acquired the strong motion data and performed the ground investigation. AK, HM, and YT participated in the reconnaissance survey of the seismic damage. HM, YT, and MA participated in the discussion and the interpretation. All authors read and approved the final manuscript.

Author details

[1] Graduate School of Engineering, Osaka University, 2-1 Yamada-oka, Suita, Japan. [2] Research and Development Center, Chodai Co., Ltd., 730 Higashi-hiratsuka, Tsukuba, Japan. [3] Graduate School of Science and Technology, Kumamoto University, 2-39-1 Kurokami, Chuo Ward, Kumamoto, Japan. [4] Graduate School of Engineering, Tohoku University, 6-6-06 Aoba, Aramaki, Aoba Ward, Sendai, Japan. [5] Graduate School of Engineering, Kyoto University, Kyoto Daigaku-Katsura, Nishikyo Ward, Kyoto, Japan. [6] School of Creative Science and Engineering, Waseda University, 3-4-1 Okubo, Shinjuku Ward, Tokyo, Japan.

Acknowledgements

The authors thank the anonymous residents of Nishi Ward, Kumamoto City for generously cooperating in conducting the temporary earthquake observations and the ground investigation. The authors also appreciate the assistance of Mr. Fumihiro Minato, a graduate student of Osaka University, during the observation. This study was carried out as an activity of the Subcommittee on Earthquake Damage Survey [Head: Associate Prof. Yoshikazu Takahashi (Kyoto University)] and the Subcommittee on Performance-based Seismic Design Method for Bridges [Head: Dr. Masaaki Yabe (Chodai Co., Ltd)], organized by the Earthquake Engineering Committee, Japan Society of Civil Engineers (JSCE) [Chairperson: Prof. Sumio Sawada (Disaster Prevention Research Institute (DPRI), Kyoto University)]. The manuscript was significantly improved based on comments from anonymous reviewers and Dr. Haruo Horikawa (guest editor).

Competing interests

The authors declare that they have no competing interests.

Received: 11 July 2016 Accepted: 19 November 2016
Published online: 01 December 2016

References

Aoi S, Kunugi T, Fujiwara H (2004) Strong-motion seismograph network operated by NIED: K-NET and KiK-net. J Jpn Assoc Earthq Eng 4(3):65–74. doi:10.5610/jaee.4.3_65

Boore DM (1983) Stochastic simulation of high-frequency ground motions based on seismological models of the radiated spectra. Bull Seismol Soc Am 73(6A):1865–1894. http://www.bssaonline.org/content/73/6A/1865.abstract

Hata Y, Nozu A, Ichii K (2011) A practical method to estimate strong ground motions after an earthquake based on site amplification and phase characteristics. Bull Seismol Soc Am 101(2):688–700. doi:10.1785/0120100142

Hata Y, Ichii K, Nozu A (2012) Three-dimensional non-linear FEM analysis of a seismic induced crack at an airport runway. Soil Dyn Earthq Eng 42:105–118. doi:10.1016/j.soildyn.2012.06.009

Hata Y, Ichii K, Nozu A, Maruyama Y, Sakai H (2013) Ground motion estimation at the farthest liquefaction site during the 2011 off the Pacific coast of Tohoku Earthquake. Soil Dyn Earthq Eng 48:132–142. doi:10.1016/j.soildyn.2013.01.002

Hata Y, Nozu A, Ichii K (2014) Variation of earthquake ground motions within very small distance. Soil Dyn Earthq Eng 66:429–442. doi:10.1016/j.soildyn.2014.08.006

Hata Y, Goto H, Yoshimi M (2016a) Preliminary analysis of strong ground motions in the heavily damaged zone in Mashiki Town, Kumamoto, Japan, during the main shock of the 2016 Kumamoto Earthquake (*MW* 7.0) observed by a dense seismic array. Seismol Res Lett 87(5):1044–1049. doi:10.1785/0220160107

Hata Y, Kataoka S, Nozu A (2016b) Accuracy of methods to estimate strong ground motions using nearby strong motion records: the equivalent linear method versus the site effect substitution method. J Jpn Assoc Earthq Eng (Jpn Engl Abstr) 16(4):195–214. doi:10.5610/jaee.16.4_195

Hata Y, Yabe M, Kasai A, Matsuzaki H, Takahashi Y, Akiyama M (2016c) Evaluation of site amplification factors at the bridges damaged by the 2016 Kumamoto earthquake sequence based on temporary earthquake observation. In: Proceedings of the 19th symposium on performance-based seismic design method for bridges. Tokyo (in Japanese) JSCE, pp 127–134

Hata Y, Murata A, Miyajima M (2016d) An approach on strong motion estimation in Kumamoto Castle during foreshock and main shock of the 2016 Kumamoto Earthquake: evaluation of site amplification factors at sites of seismic observation station by JMA. In: Proceedings of the 55th national conference of Japan landslide society, Kochi (in Japanese), pp 252–253

Horika K (2013) Clarification of mechanism of Shinkansen derailment in the 2011 Great East Japan Earthquake and countermeasures against earthquakes. JR EAST Tech Rev 27:13–16. https://www.jreast.co.jp/e/development/tech/pdf_27/Tec-27-13-16eng.pdf

Japan Meteorological Agency (2016) Monthly report on seismic and volcanic activities in June 2016. JMA Press Release on 8 July **(in Japanese)**. http://www.jma.go.jp/jma/press/1607/08a/1606jishin.html

Kato K (2001) Evaluation of source, path, and site amplification factors from the K-NET strong motion records of the 1997 Kagoshima-Ken-Hokuseibu earthquakes. J Struct Constr Eng (Jpn Engl Abstr) AIJ 543:61–68. http://ci.nii.ac.jp/naid/110004304043

Kumamoto Prefecture (2015) Regional disaster prevention plan in Kumamoto Prefecture: edition for countermeasures against earthquake and tsunami disasters. **(in Japanese)**

Ministry of Land, Infrastructure, Transport and Tourism (2016) Disclosure paper on 13th Shinkansen derailment countermeasure conference. MLIT Press Release on 25 May. **(in Japanese)**. http://www.mlit.go.jp/report/press/tetsudo07_hh_000101.html

Nakaaki S, Sakai K, Murono Y (2012) A comparative study on characteristics of earthquakes in 2011 Tohoku-Pacific Ocean Earthquake. J Struct Eng Earthq Eng (Jpn Engl Abstr) JSCE 68(4):161–168. doi:10.2208/jscejseee.68.I_161

Nishimae Y (2004) Observation of seismic intensity and strong ground motion by Japan meteorological agency and local governments in Japan. J Jpn Assoc Earthq Eng 4(3):75–78. doi:10.5610/jaee.4.3_75

Nozu A, Nagao T, Yamada M (2007) Site amplification factors for strong-motion sites in Japan based on spectral inversion technique and their use for strong-motion evaluation. J Jpn Assoc Earthq Eng (Jpn Engl Abstr) 7(2):215–234. doi:10.5610/jaee.7.2_215

Nozu A, Nagao T, Yamada M (2009) Simulation of strong ground motions using empirical site amplification and phase characteristics: modification to incorporate causality. J Struct Eng Earthq Eng (Jpn Engl Abstr) JSCE 65(3):808–813. doi:10.2208/jsceja.65.808

Ogura M (2006) The Niigata Chuetsu earthquake: railway response and reconstruction. Railw Transp Rev 43/44:46–63. http://www.ejrcf.or.jp/jrtr/jrtr43_44/pdf/f46_ogu.pdf

Railway Technical Research Institute (1999) Specifications for railway structures and commentary: seismic design edition. Maruzen Co. Ltd, Tokyo **(in Japanese)**

Railway Technical Research Institute (2012) Specifications for railway structures and commentary: seismic design edition. Maruzen Co. Ltd, Tokyo **(in Japanese)**

Senna S, Adachi S, Ando H, Araki T, Iisawa K, Fujiwara H (2006) Development of microtremor survey observation system. Japan Geoscience Union Meeting, Makuhari, Japan (in Japanese), pp 14–18. http://ci.nii.ac.jp/naid/10018357183

Suzuki W, Iwata T (2006) Source model of the 2005 west off Fukuoka Prefecture earthquake estimated from the empirical Green's function simulation of broadband strong motions. Earth Planets Space 58(1):99–104. doi:10.1186/BF03351921

Tokunaga M, Sogabe M, Tanimura H, Kiyoshi O (2015) Method for evaluating equivalent natural period with microtremor measurement. J Struct Eng Earthq Eng (Jpn Engl Abstr) JSCE 71(1):72–86. doi:10.2208/jscejseee.71.72

Uehara H, Kusakabe T (2004) Observation of strong earthquake motion by National Institute for Land and Infrastructure Management. J Jpn Assoc Earthq Eng 4(3):90–96. doi:10.5610/jaee.4.3_90

Yasuda S, Yamaguchi I (1985) Dynamic soil properties of undisturbed samples. In: Proceedings of the 20th annual Japan geotechnical society (JGS) conference (in Japanese), pp 539–542

Yoshida N, Kobayashi S, Suetomi I, Miura K (2002) Equivalent linear method considering frequency dependent characteristics of stiffness and damping. Soil Dyn Earthq Eng 22(3):205–222. doi:10.1016/S0267-7261(02)00011-8